Sinuous Flow in Cutting of Metals

Ho Yeung,[1,*] Koushik Viswanathan,[1] Anirudh Udupa,[1] Anirban Mahato,[2] and Srinivasan Chandrasekar[1]
[1]*Center for Materials Processing and Tribology, Purdue University, West Lafayette, Indiana 47907, USA*
[2]*Department of Mechanical Engineering, Indian Institute of Technology, Patna 801106, India*
(Received 20 June 2017; revised manuscript received 17 September 2017; published 22 November 2017)

Using *in situ* high-speed imaging, we unveil details of a highly unsteady plastic flow mode in the cutting of annealed and highly strain-hardening metals. This mesoscopic flow mode, termed sinuous flow, is characterized by repeated material folding, large rotation, and energy dissipation. Sinuous flow effects a very large shape transformation, with local strains of ten or more, and results in a characteristic mushroomlike surface morphology that is quite distinct from the well-known morphologies of metal-cutting chips. Importantly, the attributes of this unsteady flow are also fundamentally different from other well-established unsteady plastic flows in large-strain deformation, like adiabatic shear bands. The nucleation and development of sinuous flow, its dependence on material properties, and its manifestation across material systems are demonstrated. Plastic buckling and grain-scale heterogeneity are found to play key roles in triggering this flow at surfaces. Implications for modeling and understanding flow stability in large-strain plastic deformation, surface quality, and preparation of near-strain-free surfaces by cutting are discussed. The results point to the inadequacy of the widely used shear-zone models, even for ductile metals.

DOI: 10.1103/PhysRevApplied.8.054044

I. INTRODUCTION

The cutting of metals involves material removal in the form of a chip by a sharp tool interacting with a workpiece (Fig. 1). Chip formation in ductile metals is typically continuous and occurs by intense shear deformation, with strains of 1–10 that are confined to a narrow region—the deformation zone. The thickness of the cut chip (h_C) is substantially greater than the undeformed chip thickness (h_0). This shape transformation of the workpiece material into the chip is commonly envisaged as occurring by simple shear, within the framework of metal plasticity [1]. On this basis, the principal features of chip formation are described by a model proposed independently by Merchant [2] and Piispanen [3] nearly 75 years ago, wherein the shear deformation is idealized as occurring on a plane—the shear plane (Fig. 1). Variants of the model consider the deformation as being spread out over a zone (a "shear zone") of small width instead of a plane [4,5]. The shear-plane and shear-zone models both rely on the fundamental assumption of steady laminar material flow to use a fluid mechanical analogy during deformation. This flow is characterized by parallel streaklines and minimal material rotation. A natural consequence of laminar flow is homogeneous deformation and uniform microstructure in the chip.

An important exception to the laminar-flow picture has also been recognized for some time, pertaining to flow localization by shear banding (e.g., in Ti, Mg, and Ni systems) [6–9]. Shear-band flow is highly nonuniform (nonlaminar) and characterized by a chip with a sawtooth morphology, wherein small bands of intense strain are separated by larger blocks of a much-less-strained material [1,10–12]. The common mechanism for shear banding is the competition between strain or strain-rate hardening and temperature-induced softening leading to intense flow localization [10,13]. This localization, usually observed

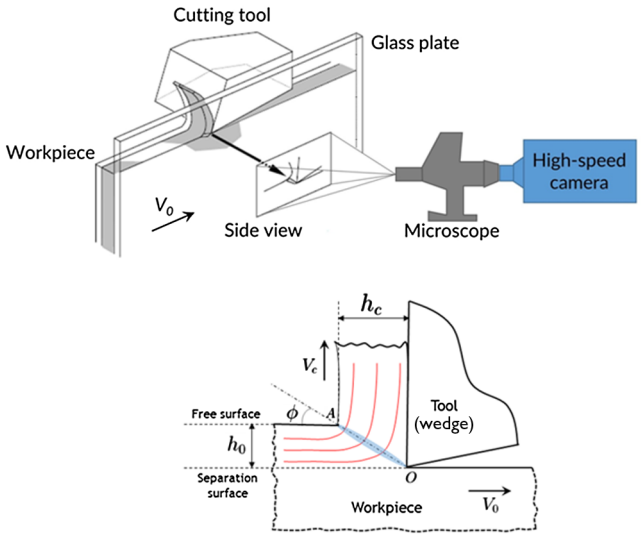

FIG. 1. Schematic of plane-strain cutting. (Top row) Experimental setup showing a tool-workpiece interaction and a high-speed imaging system. (Bottom row) Side view showing the plane of deformation. The workpiece material is deformed by the tool into a chip, here depicted as occurring by smooth laminar flow (the red lines) with shear concentrated in a narrow shear plane or zone (shown in blue).

[*]Present address: National Institute of Standards and Technology, Gaithersburg, MD, USA.

in cutting under extreme deformation rates (e.g., high speeds), clearly negates the fundamental assumption of smooth laminar flow [10]. Shear banding produces undesirable consequences for the machining process such as fluctuating forces, poor surface finish, chatter-type conditions, and nonuniform properties on the cut workpiece surface [10,14].

In light of these observations, there has been debate over what determines the mode of flow, particularly when, as in cutting, the strains are large, and the deformation zone is unconstrained and close to a free surface. Beginning with Hill's analyses of shear-plane stability in a rigid perfectly plastic solid [15,16], several hypotheses have been put forth, ranging from dependence on deformation geometry to a material deformation response [17]. These analyses have, however, largely been carried out with the basic model of a perfectly plastic material (no strain hardening) and have postulated laminar flow, so that the question of what types of unsteady (nonlaminar) flow can occur has remained largely unanswered.

The problem regarding nonlaminar flows and flow instability has received fresh impetus with the recent uncovering of an unsteady deformation mode—sinuous flow—in the cutting of annealed metals (with a high strain-hardening capacity), even under small deformation rates (1–10 mm/s) [18]. This discovery occurred during re-examination, using *in situ* observational techniques, of a surprising, and long-known, observation, that soft annealed metals are much more difficult to cut than the same metals in an initially hardened state. While chip formation is continuous in both cases, the cutting of the annealed metal produces an unusually thick chip and large forces: the deformed chip thickness h_C can be as much as 10 to 15 times the undeformed value h_0 (Fig. 1), indicative of very large plastic strains [11,18–20]—and, hence, large forces. The usual explanation of this phenomenon has invoked laminar plastic flow with high tool-chip friction, coupled with the shear-plane or -zone model, to explain the large chip thickness (shape) change. However, thickness changes of $10\times$–$15\times$ by simple shearing are anomalously large and are not known to occur anywhere else in a single stage of homogeneous deformation. It is also difficult to explain the resulting chip morphology, characterized by irregular mushroomlike features on the chip back surface [14,19,21,22], within the framework of laminar flow. The *in situ* observations revealed that this large chip shape transformation occurred by sinuous flow—a highly unsteady flow with strain heterogeneity [18]. Since the laminar-flow model should work best for highly ductile materials like annealed metals [2,5], these observations pertaining to sinuous flow and material folding have raised fresh doubts about the well-accepted smooth-flow models of chip formation.

In this study, with the objective of better understanding unsteady flows in large-strain deformation, we analyze the cutting of highly strain-hardening metals in detail using high-speed *in situ* imaging and image analysis. We study sinuous flow development—conditions for occurrence, its nucleation and propagation phases, its characteristics, and the energy for effecting shape change—using copper, aluminum, and brass as model material systems and at small deformation rates. Sinuous flow is confirmed to be a general flow mode in annealed metals, a mesoscopic deformation mode in the same genre as kinking [23] and shear banding [7,10], and with the capability to effect large shape changes. We highlight the principal factors that influence this flow development and outline a phenomenological mechanism for its cause. It is shown that a simple shear of annealed metals to large plastic strains is highly, and intrinsically, nonuniform at the mesoscale and cannot be described in the framework of laminar flow. Implications for the role of stability of plastic deformation in selecting the flow mode in cutting, along with the preparation of high-quality surfaces in metals, are discussed. The results also point to the inadequacy of the 70-year-old shear-zone models for the cutting of highly ductile metals.

II. EXPERIMENTAL PROCEDURES

The experimental system for studying large-strain deformation consists of a metal-plate workpiece ($50\times25\times3$ mm), moving against a fixed-wedge tool (Mo-Max M42 high-speed steel) at constant speed V_0 under conditions of plane strain (2D); see Fig. 1. The temperature rise in the deformation zone is negligible at these low speeds, which correspond to small nominal deformation rates (1–100 s^{-1}). A unique feature of this configuration is the capability to impose large plastic strains by simple shear. The undeformed and final chip thicknesses are denoted h_0 and h_C, respectively. Typical h_0 values used are 50–100 μm, much greater than the tool cutting-edge radius of approximately 5 μm. The tool rake face is fixed normal to V_0, as in Fig. 1 (bottom panel), so that the rake angle $\alpha = 0°$; this model mimics many natural and industrial cutting processes [1,24]. Side flow during deformation is prevented by using a clamped glass block, thereby ensuring plane-strain deformation.

The workpieces are made of 99.99% oxygen-free high-conductivity (OFHC) copper (alloy 101, McMaster-Carr) and commercially pure aluminum (Al 1100). The Cu samples are annealed in air at 750 °C for 4 h and oven cooled to room temperature. The average grain size is approximately 500 μm after annealing, and the hardness is 68 HV (Vickers pyramid number). The Al samples are annealed similarly, with an initial postannealing grain size of about 400 μm and a hardness of 30 HV. The workpiece surface being cut is carefully prepared so as to ensure that their initial deformation state is well defined [18]. The surface roughness after this preparation is approximately 0.1 μm Ra (the arithmetic average of the roughness profile).

All cutting is performed with the workpiece at room temperature ($T = 300$ K, $T \ll 0.5T_m$, where T_m is the workpiece melting temperature) and with continual application of Mobil 1 5W-30 lubricant. Some cutting experiments are also done with single-phase (70-30) brass.

A series of experiments is carried out at $V_0 \leq 10$ mm/s, in which the flow of metal during the cutting is observed *in situ* using a high-speed CMOS camera (pco.dimax) coupled to an optical microscope (Nikon Optiphot), with framing rates of up to 5000 frames/s. The imaging configuration provides for a spatial resolution of 1.4 μm per pixel and sensor recording areas as large as 1296×1296 pixels. The images are postprocessed using particle image velocimetry (PIV), an image-correlation technique, to obtain a comprehensive quantitative record of displacement, velocity, and effective (von Mises) strain rate and strain fields [18,25]. The PIV technique and its variants have been widely used in fluid and solid mechanics for characterizing flows [25,26]. Streaklines and path lines [27] of flow are constructed from the velocity field data, enabling analysis of phenomenological aspects of the flow, including flow nonhomogeneity and the onset of instability.

A second series of experiments at higher speeds, $V_0 = 10$–60 mm/s, is conducted with the tool being fed radially into a rotating disk workpiece. Plane strain conditions akin to Fig. 1 are realized by an appropriate selection of h_0, and by constraining the disk workpiece between similar metal disks clamped onto both of its faces. The deformation zone is observed *in situ* using a high-speed imaging system, as with the linear cutting. A third series of cutting experiments is performed to analyze how the initial hardening affects material flow and chip characteristics. This involves cutting Cu and Al workpieces in different initial hardened states. The initial hardening is effected either by rolling or by sliding against a steep-angled wedge (large $\alpha = -70°$). The latter is especially useful for imposing large prestrains (>2) on a surface layer of depth greater than the uncut chip thickness (i.e., $> h_0$). The initial strain imposed is measured by PIV (sliding) or estimated from dimensional changes (rolling).

A high-frequency piezoelectric dynamometer (with a natural frequency of 2 kHz; Kistler 9272) attached to the tool assembly is used to measure the cutting force (the force in the direction of V_0) at a sampling rate of 1 kHz. The forces are correlated with the optical images and provide complementary information on material flow. The force data are also used to estimate the specific energy of chip formation and assess flow characteristics. The workpiece regions in the vicinity of the flow zone and the deformed chip are characterized by optical metallography, scanning electron microscopy (SEM), and stylus profilometry to analyze microstructural and topographical features, and to obtain additional flow information.

III. RESULTS

The *in situ* observations reveal that sinuous flow is a dominant deformation mode in the cutting of annealed metals. An analysis helps us to establish the principal characteristics of this flow and key aspects of the flow development.

A. Sinuous flow and its characteristics

The main features of the sinuous flow may be illustrated using observations from the cutting of annealed Cu; see Fig. 2(a). Derived from a high-speed image sequence, this frame shows the flow in effecting shape transformation of the workpiece material into the chip. The material deformation is revealed by streaklines, which are characterized by periodic wavy patterns and significant vorticity; this type of highly unsteady flow is termed sinuous flow [18]. The chip forms by repeated folding over of the incoming workpiece material. This folding, highlighted by the streaklines, is extensive, with fold amplitudes often being as much as one half to two thirds of the thickness of the chip (h_C). The temporal fold frequency corresponding to Fig. 2(a) is 1.7 Hz. The sinuous-flow pattern bears little resemblance to anything hitherto reported in classical plasticity. It is radically different from the laminar flow of the shear-plane model of cutting (Fig. 1) and the highly localized flow that typifies shear banding in the large-strain deformation of metals.

The effective (von Mises) strain field ($\dot{\epsilon}$) in the Cu chip derived from PIV is shown as background color in Fig. 2(a).

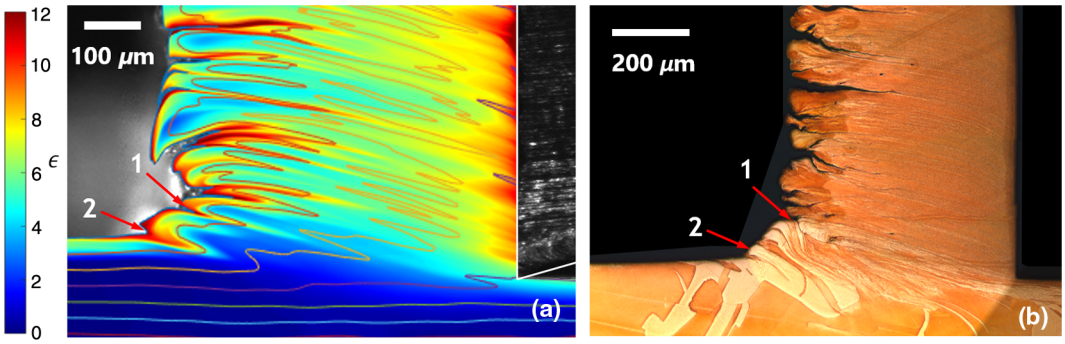

FIG. 2. Sinuous flow in Cu. (a) Image from a high-speed sequence with overlaid streaklines and strain field. Repeated material folding is revealed by the streakline pattern. (b) Postmortem micrograph shows mushroomlike structures (as between 1 and 2) that are characteristic of sinuous flow.

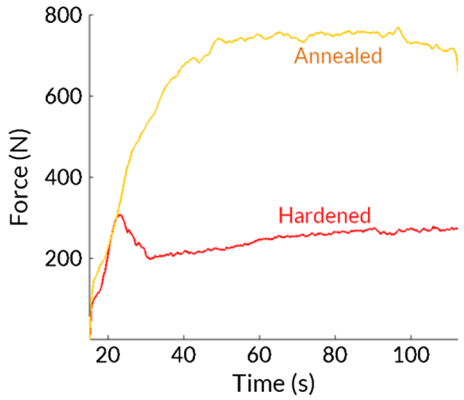

FIG. 3. Cutting forces reflect the mesoscopic flow mode in Cu. The force for cutting annealed Cu via sinuous flow (the yellow line) is much larger (3×) when compared to cutting the same material in an initial hardened state (the red line).

The sinuous flow causes an inhomogeneous strain distribution in the chip interior, with the effective strain fluctuating between 4 and 8. A representative value of 5.6 is obtained for the chip strain based on volume-weighted averaging of the strain field. The strain oscillations reflect the fold development and the structural inhomogeneity that underlie the flow.

Figure 2(b) is an optical microscope picture of the Cu chip showing its meso- and macroscale structure. The macrostructure shows that the chip, essentially of constant thickness, has singular mushroomlike formations on its free surface as a consequence of the repeated folding. This morphology is quite different from the sawtooth structure of shear-banded chips [10–12]. Furthermore, the chip is very thick, $h_C \sim 14h_0$. This extraordinary thickening is a consequence of the sinuous flow—it is nearly impossible to envisage such a large shape change within the framework of laminar flow, despite many such theoretical claims [11,19,21].

Neither the strain fluctuations in the chip nor the morphological structural (mushroom) heterogeneity is reflected in the cutting force (Fig. 3). The measured force in the annealed Cu shows no decipherable oscillations at anywhere near the fold frequency of 1.7 Hz, even though this frequency is well within the measurement resolution of the sensor (500 Hz). The extent of the strain variation due to sinuous flow, both spatially and in magnitude, is much less severe than in shear banding under adiabatic deformation conditions [10]. In the latter case, the ratio of the maximum strain (shear-band strain) to minimum strain (strain between the bands) is often >10 and, furthermore, the regions of high strain are extremely localized, on the order of a few micrometers in the chip [12]. For the purpose of comparison, Fig. 3 also shows the force while cutting the same metal (Cu) in the hardened state. Here, prior observations have confirmed that folding is absent [18], and that the deformation occurs by laminar flow. As a result, the forces are much lower.

In addition to Cu, sinuous flow is observed in the cutting of other annealed metals, such as aluminum and (single-phase) brass 260. Figure 4(a) shows streakline profiles from the cutting of annealed Al, showing the same distinguishing characteristics—material rotation, repeated folding, self-contacts, and the mushroomlike morphology of the chip surface (marked with an arrow). The chip strain distribution is inhomogeneous [Fig. 4(b)], as in the Cu case, with alternating regions of high and low strain. The thickness of the Al chip is $h_C \sim 9h_0$ (compared to $h_C \sim 14h_0$ in the Cu case). This is the case because the extent of the folding in Al is smaller, as can be inferred by comparing the streakline amplitudes in Figs. 4(a) and 2(a). The reduced folding is reflected in a somewhat weaker heterogeneity in the Al strain field [Fig. 4(b)] than in the Cu one [Fig. 2(a)]. The maximum strain in the Al case is 4.5, compared to 8 in the Cu example.

The folds are observed to occur across the entire chip width (Fig. 5) and cause the mushroomlike structures (the arrows extending from A). Absent the present *in situ* observations, it is clear that the occurrence of sinuous flow cannot be inferred solely from postmortem chip structure observations of the type shown in Figs. 2(b) and 5. Consequently, mushroom structures have previously been thought, erroneously, to arise from smooth laminar flow modulated by periodic cracking on the chip free

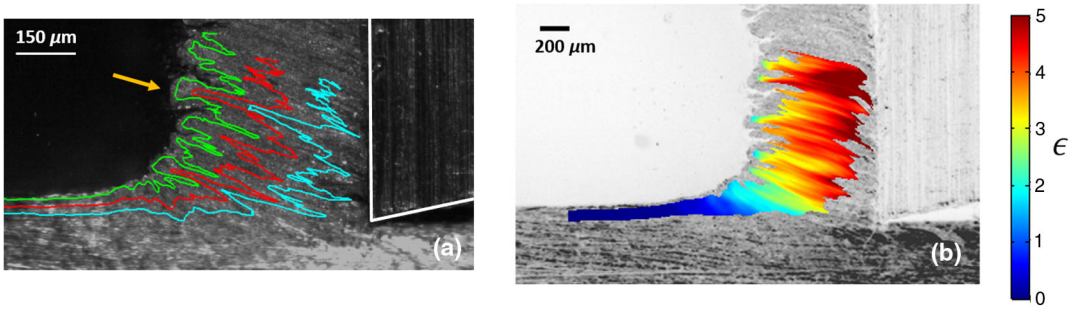

FIG. 4. Sinuous flow in Al. (a) Image taken from a high-speed sequence with overlaid streaklines track material flow in the vicinity of the tool. Multiple folds are observed (such as at the arrow) stacked over one another in the chip. (b) The strain distribution is correspondingly inhomogeneous, with alternating regions of low and high strain in each fold.

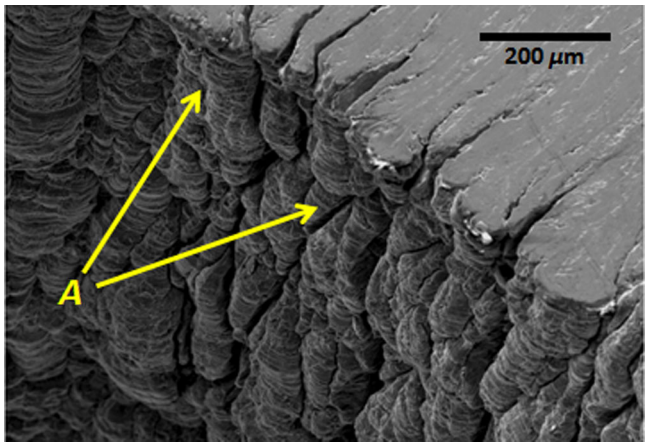

FIG. 5. SEM image of an Al chip (back) surface showing folds (the arrows coming from A) extending across the entire chip width.

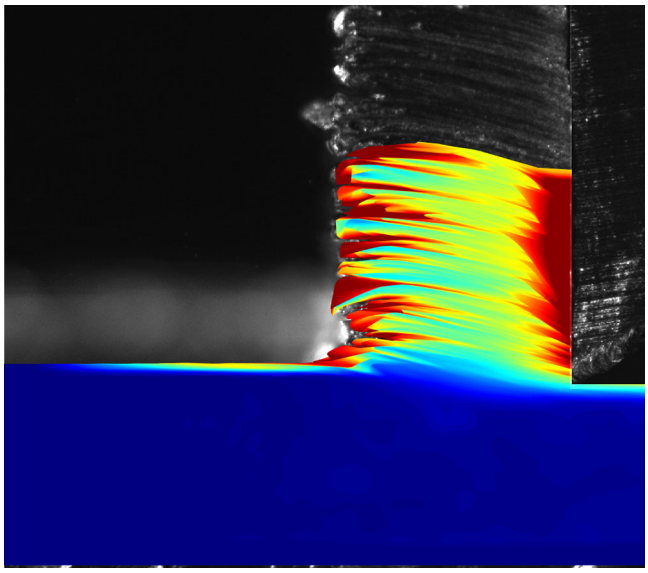

VIDEO 1. Development of heterogeneous strain field in the chip due to repeated material folding.

surface [11,19]. The present observations establish mushroom structures as an unambiguous signature of sinuous flow resulting from material folding and not cracking. Based on this correlation, sinuous flow appears to be quite widespread in the cutting of annealed metals, including low-carbon steels and iron [19,21,28], in addition to the Cu, Al, and brass discussed herein.

B. Development of sinuous flow

The observations have shown that repeated material folding is responsible for the sinuous flow, necessitating a detailed understanding of the folding process. Each fold-formation event is initiated by the formation of a bump on the workpiece surface just ahead of the advancing tool. The three frames in Fig. 6, taken from a high-speed image sequence, show the formation of the bump and its evolution into a fold in annealed Cu. The color scheme depicts the underlying strain field, obtained from PIV. Video 1 shows a development of the heterogeneous strain field in the chip. The initial bump in Fig. 6(a) is bounded by two points, P_1 and P_2, likely grain boundaries, which act as local pinning points. They force the bump to deform plastically, resulting in a pronounced bulge on the free surface in Fig. 6(b). A white dotted line—the bump axis—joins the peaks of adjacent streaklines, indicating the orientation of the impending fold. The bump axis is nearly parallel in both frames. Simultaneously, the workpiece material also imparts a constant vertical velocity as it is constantly forced against the vertical tool face. The bump in

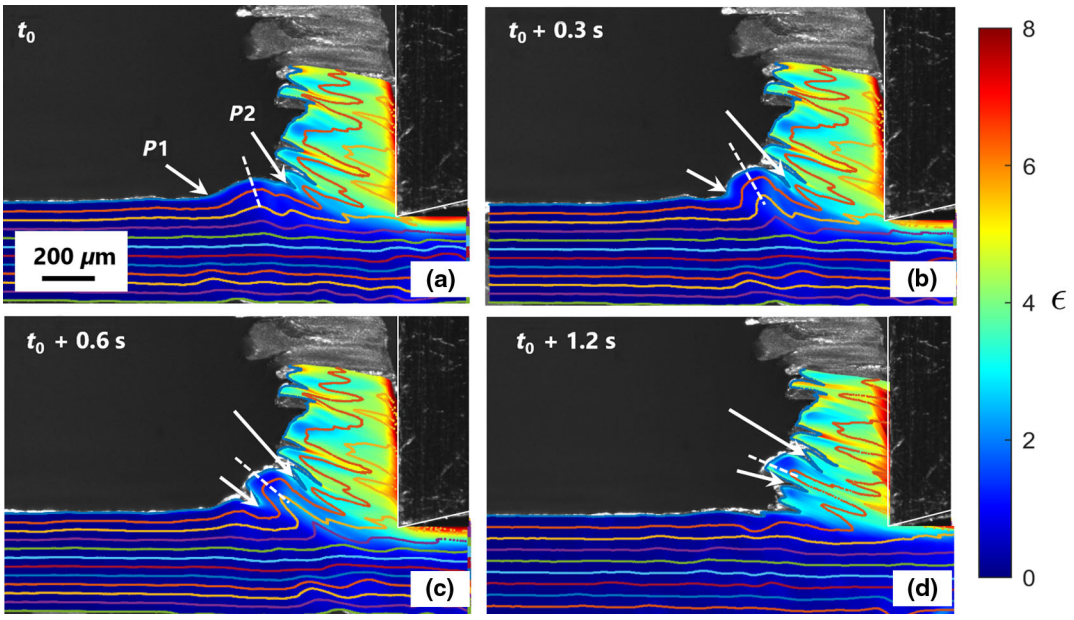

FIG. 6. Development of individual folding events leading to sinuous flow in Cu. Four frames from a high-speed sequence show the fold nucleation process. (a) A bump is formed on the free surface due to local material buckling between pinning points P_1 and P_2. (b),(c) The bump axis (the dashed line) rotates as material is continuously sheared. (d) The shearing and rotation is now complete, finally resulting in a fold in the chip.

Fig. 6(b) is thereby sheared, causing the axis to rotate in a counterclockwise direction. As the material nears the tool face, the shear increases, and the bump is consequently amplified while also reducing its original width [Fig. 6(c)]. The material between P_1 and P_2 now constitutes a single fold. Folding is complete [Fig. 6(d)] once the original bump axis is rotated by nearly 90°, at which time another bump is initiated ahead of the tool face and the process repeats.

The fold nucleation process, along with bump formation, is reminiscent of the plastic buckling of a column under axial compression [29], which is discussed in more detail in Sec. IV A. This nucleation and evolution process is a consistent feature of sinuous-flow development, confirmed by similar observations in the cutting of annealed Al [Fig. 7]. Here, as in the Cu case, the first bump is initiated ahead of the chip [the yellow arrow in Fig. 7(a)], then undergoes shear and rotation as it traverses the deformation zone to form a fold. The chip is once again composed of a series of folds [the blue and yellow arrows in Fig. 7(d)].

C. Fold attributes

The streaklines, in addition to directly revealing the material folding, contain quantitative information about the folds. This information is extracted using fold analysis methods borrowed from structural geology [30] and is summarized in Fig. 8. The data are based on streaklines taken at steady state; hence, the results are unchanged by time translation. As background for interpreting these results, consider two streaklines that are schematically depicted (in orange and green) in the inset to Fig. 8(a). The curvature of each streakline is evaluated to locate the two minima (M_1, M_2) and the intermediate maximum (P) bounding a single fold. The maxima of two successive streaklines are denoted P and P', and the midpoint of the line M_1M_2 is M. The angles ϕ and θ, subtended by PP' (also called the bump axis) and PM with the horizontal, are a measure of the rotation of a layer of material and of a single streakline, respectively. A large difference between ϕ and θ means a sharp gradient in material deformation between the two successive streaklines. The fold amplitude A and width W are defined as the lengths PM and M_1M_2, respectively.

Figure 8(a) shows the distribution of fold widths along the chip in the cutting of Cu. This distribution reflects the underlying material microstructure. First, all fold widths are less than the initial nominal grain size (500 μm), consistent with a grain-based origin of fold nucleation [18,25,31]. Second, the ratio of initial grain size (about 500 μm) to mean fold width (approximately 50 μm) is roughly equal to the chip-thickness ratio (h_C/h_0), indicating that, on average, each fold is formed by the deformation of a single grain. Third, a large distribution of fold widths (showing a standard deviation of 30 μm) is seen, likely reflecting the grain-size distribution in the Cu case.

The severity of material deformation in each fold, as a function of the depth from the chip back surface, is shown in Fig. 8(b). Here, the deformation severity is reflected in a small layer thickness (length PP'), as depicted for three consecutive streaklines. In the first streakline, which is closest to the free surface (red), this layer thickness is very small and comparable to the fold width (about 50 μm). This small thickness is due to the severe deformation in the vicinity of the free surface. Further from the surface, in streaklines 2 (green) and 3 (blue), there is an increase in layer thickness, which is consistent with a reduction in deformation. The rotation that a fold undergoes in the deformation zone is shown in Fig. 8(c), where the angles ϕ and θ are plotted against each other. For folds with little

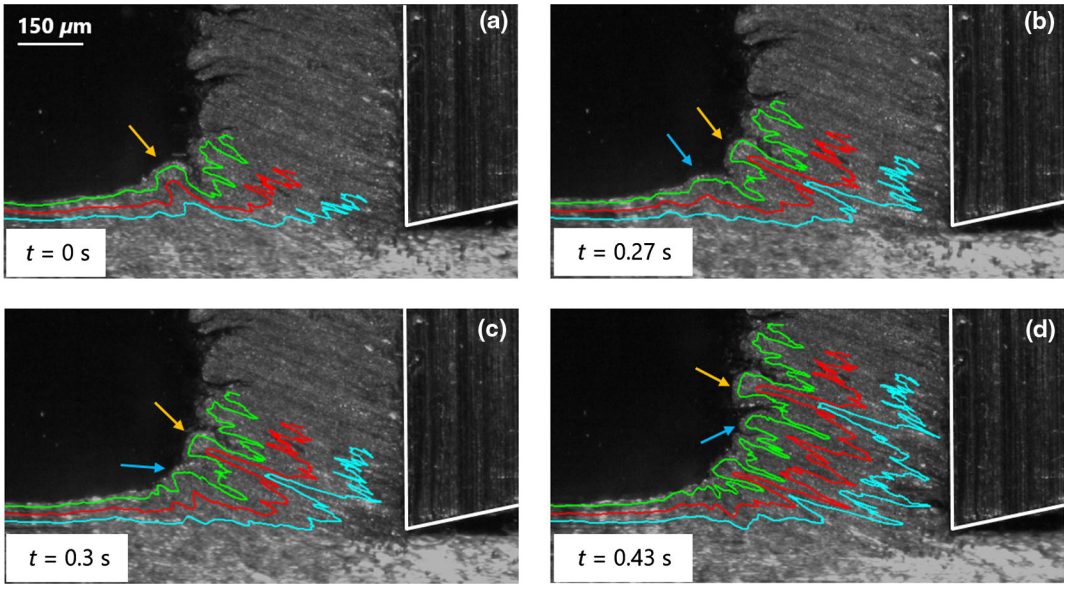

FIG. 7. Sinuous-flow development in Al. (a) Fold nucleation occurs due to material buckling (the yellow arrow) on the free surface ahead of the tool. (b),(c) Rotation and collapse of adjacent folds in the chip (the blue and yellow arrows) resulting in (d) the characteristic mushroom shape on the back side of the chip.

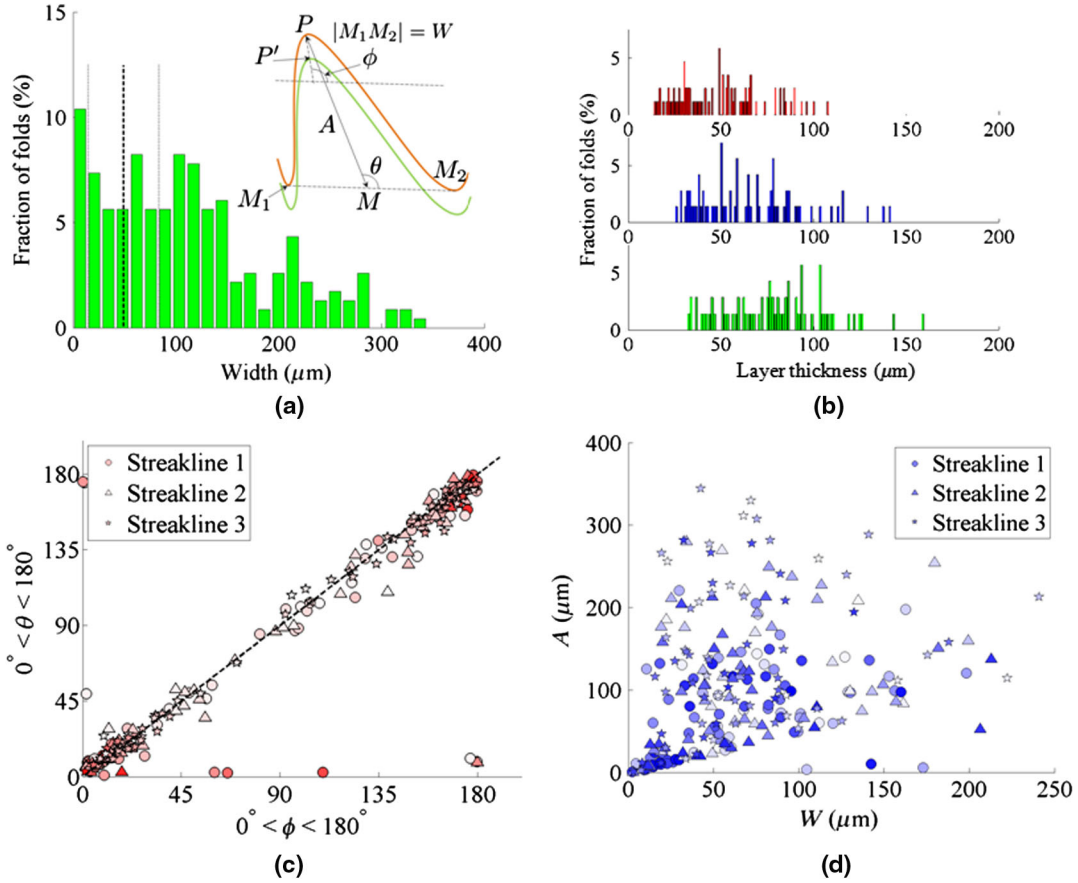

FIG. 8. Fold properties and statistics in annealed Cu based on streakline data at steady state. (a) Distribution of fold widths along the chip shows a correlation with the material grain size. The dashed and dotted lines represent the mean and one standard deviation of fold width. (Inset) Schematic of a single fold as depicted by two streaklines (in orange and green). The peaks of these streaklines are at P and P', respectively. The fold minima are at M_1 and M_2, and M is the midpoint of M_1M_2. The amplitude A and the width W are taken. ϕ and θ are the angles subtended by the lines PP' and PM with the horizontal. (b) Histogram plot of thickness (equal to length PP') of folds for the first (red), second (blue), and third (green) streaklines from the free surface. Intense folding near the surface is reflected in low layer thickness. (c) Variation of ϕ vs θ shows that the two are nearly equal for each fold in all three streaklines. Folds with the highest widths (in red) have $\phi, \theta = 0°$ or 180° (acutely sheared). (d) Distribution of W vs A for folds along streaklines 1, 2, and 3. Incipient folds (the white markers) show a wide distribution of A, W, but a much narrower distribution is observed for fully developed folds (in blue).

material shear and a small rotation gradient, ϕ and θ should lie along the 45° line (which is dashed). The scatter points are color coded as a function of fold width, with the large widths in red and the small ones in white. Clearly, the larger folds are also the ones that are most acutely sheared ($\phi, \theta \simeq 0°, 180°$) while the smaller folds (shown in white) remain upright ($\phi, \theta \simeq 90°$). Last, the evolution of folds is ascertained by tracking the fold amplitude A vs width W for the three streaklines; see Fig. 8(d). The incipient folds corresponding to bump formation in Fig. 6 are depicted in white, while the folds in the chip after a large deformation are shown in blue. Initially, a wide distribution of A and W values is observed, which is consistent with the grain-size distribution and bump-initiation mechanism outlined. As deformation progresses, A and W tend to fall into a narrow triangular zone with hardly any folds having high A and low W values, or vice versa.

D. Energy dissipation in flow

The energy dissipated in large-strain deformation can be obtained from both the measured (PIV) strain field and the forces. We now present these independent estimates of the energy that provide insight into the stability of sinuous flow *vis-à-vis* laminar flow in annealed metals.

1. Estimate based on laminar-flow model

If the chip shape transformation is envisioned as always occurring by smooth laminar flow with a shear plane [2], then the chip shear strain can be estimated from the chip-thickness ratio ($\lambda = h_C/h_0$; Fig. 1) measurements alone, as $\gamma = \lambda + 1/\lambda$. Despite its invalidity, if we apply this laminar-flow assumption to the thick chip with annealed Cu (Fig. 2), we obtain $\gamma \sim 14.1$ and the von Mises strain $\epsilon = \gamma/\sqrt{3} = 8.1$. The specific energy (energy per unit

volume) for such a (hypothetical) shape transformation is then obtained as $U_{\rm lam} = \int \sigma d\epsilon$. The constitutive relation for flow stress (σ) in Cu is given by [32]

$$\sigma = (A + B\epsilon^n)\left(1 + C\ln\frac{\dot{\epsilon}}{\dot{\epsilon}_0}\right)\left[1 - \left(\frac{T - T_0}{T_m - T_0}\right)^m\right], \quad (1)$$

where $\dot{\epsilon}$ and $\dot{\epsilon}_0$ are the experimental and reference strain rates (in s^{-1}) and T, T_m, and T_0 are the temperature of the deforming work material, the melting temperature, and room temperature, respectively. Coefficient A is the initial flow stress (in megapascals) in a tensile test, B is the hardening modulus (in megapascals), C is the strain-rate sensitivity coefficient, n is the hardening coefficient, and m is the thermal softening coefficient.

At low cutting speed, as in the present case ($V_0 = 0.42$ mm/s), $\dot{\epsilon} \simeq \dot{\epsilon}_0$, $T \simeq T_0$, and the constitutive law simplifies to

$$\sigma = A + B\epsilon^n. \quad (2)$$

For annealed OFHC copper, $A = 90$ MPa, $B = 292$ MPa, and $n = 0.31$. The specific energy ($U_{\rm lam}$) is obtained as $U_{\rm lam} = \int_0^{\epsilon_0} \sigma d\epsilon = [A\epsilon + (B\epsilon^{n+1}/n + 1)]_0^{\epsilon_0}$, with $\epsilon_0 = 8.1$ from the chip thickness data. Substituting values for A, B and ϵ_0, we obtain $U_{\rm lam} \simeq 4.2\,{\rm J/mm^3}$.

2. *Energy from in situ flow field measurements*

The actual energy dissipation in sinuous flow can be obtained from the deformation work $\int \sigma d\epsilon$, as evaluated along the flow in the high-speed images, using the PIV strain and flow data. The incremental strain $\Delta\epsilon_{(ij)}$ at any pixel location i at frame j is used to estimate the entire strain field, i.e., $\epsilon_{(ij)} = \sum_{k=1}^{j} \Delta\epsilon_{(ik)}$. Note that i, j, and k here are not tensor indices but instead correspond to scalar strain values (effective strain) at pixel location i at frames j or k. Neglecting temperature and strain-rate effects and using the constitutive law for annealed copper [see Eqs. (1) and (2)], the flow stress and specific energies are obtained as

$$\sigma_{(ij)} = (A + B\epsilon_{(ij)}^n), \quad (3)$$

$$U_{(ij)} = \sum_{k=1}^{j} (A + B\epsilon_{(ik)}^n)\Delta\epsilon_{(ik)}. \quad (4)$$

The total energy E dissipated per unit sample width in a region at frame j is obtained by adding the contributions for all pixels i within that region. This computation for the sinuous-flow chip ($E_{\rm sin}$) and subsurface region ($E_{\rm sub}$) is shown in Fig. 9. The total energy dissipation $E_{\rm PIV} = E_{\rm sub} + E_{\rm sin}$ is found to match well with the energy value derived from the force measurement ($E_{\rm force}$).

The specific energy $U_{\rm sin}$ for chip shape transformation, obtained as $E_{\rm sin}$ divided by volume removed, given by

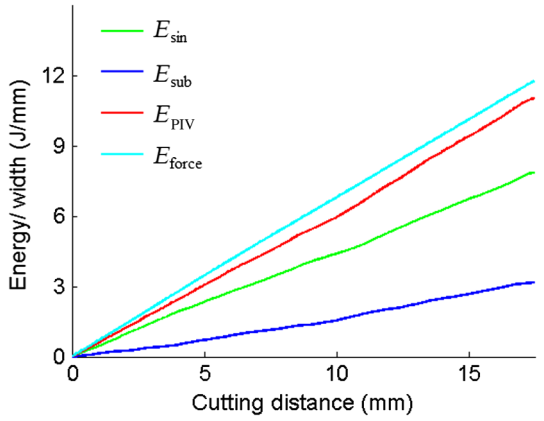

FIG. 9. Energy dissipation in sinuous flow, based on PIV calculations. The energy in the deformation process is split into the $E_{\rm sin}$ that goes into the chip due to folding, the $E_{\rm sub}$ that goes into the workpiece substrate, and the total, $E_{\rm PIV} = E_{\rm sin} + E_{\rm sub}$, that is dissipated in the cutting process. A parallel estimate obtained from force measurements ($E_{\rm force}$) matches the value of $E_{\rm PIV}$ very closely.

$U_{\rm sin} \simeq 2.9\ {\rm J/mm^3}$. It is also clear from these analyses for annealed Cu that the energy estimate for chip shape transformation based on an assumption of laminar flow ($U_{\rm lam} = 4.2\ {\rm J/mm^3}$) is larger than the actual energy dissipation ($U_{\rm sin} \sim 2.9\ {\rm J/mm^3}$) via sinuous flow, indicating that such a large shape transformation is more efficiently effected by nonlaminar flow.

E. Laminar-flow characteristics: Cutting of hardened metals

As discussed above, the cutting of highly ductile metals such as annealed Cu and Al occurs via extensive fold formation in the chip. However, when the material's propensity for strain hardening is exhausted, such as by prestraining, sinuous flow no longer occurs.

Figure 10 shows the flow field in the cutting of hardened Cu (having a prestrain of about 2) derived from PIV analysis. The smooth, nearly parallel streakline pattern [Fig. 10(a)] shows the flow to be laminar, and very different from that in the annealed Cu [Fig. 2(a)]. The strain-rate field is well defined and narrow [Fig. 10(b)], indicating that the deformation zone is highly confined. This laminar-flow field is very similar to that in the shear-plane models (see, e.g., the schematic in Fig. 1). The chip is relatively thin, and the shape change in chip formation is quite small, $h_C/h_0 \sim 2$, relative to the sinuous-flow shape transformation in annealed Cu ($h_C/h_0 \sim 14$). This reduced level of plastic deformation is reflected in the much smaller chip strain (1.5) and cutting force (200 N; Fig. 3), both of which are only about one fourth of the corresponding values measured in the cutting of annealed Cu [Figs. 2(c) and 3]. The cutting of hardened Cu by laminar flow thus involves much lower (plastic) energy dissipation than the cutting of

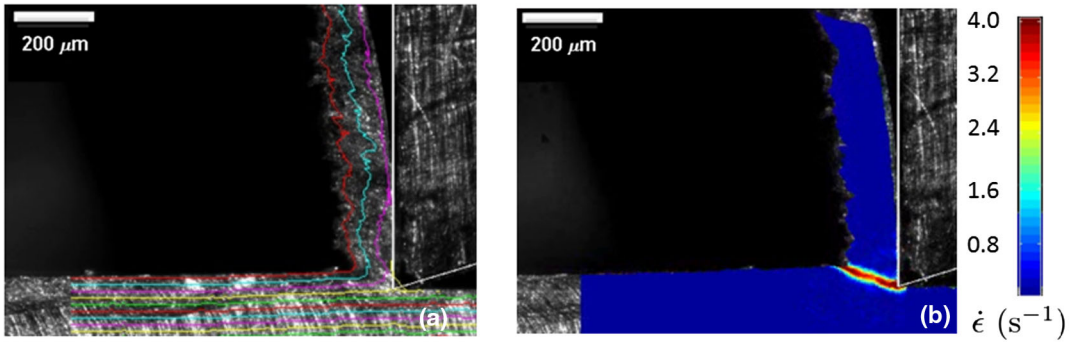

FIG. 10. Laminar flow when cutting hardened Cu, as revealed by (a) smooth streaklines and a consistent, narrow deformation zone, as indicated by (b) the strain-rate field.

annealed Cu by sinuous flow, even though the hardened Cu has an initial yield stress (400 MPa) that is nearly 4 times that of the annealed Cu (90 MPa). Similar results are obtained for the cutting of annealed and hardened Al.

F. Flow and chip-thickness oscillations

The residual plastic strain on the cut workpiece surface for sinuous (annealed Cu) and laminar (hardened-Cu) flows is depicted in Fig. 11. For the case of sinuous flow [Fig. 11(a)], a large residual strain ($\epsilon \sim 4$) is observed on the newly formed workpiece surface. As a result, the newly created workpiece surface is in a strain-hardened state. This hardened region extends to a depth approximately h_0 from the free surface. By contrast, with the laminar flow (hardened Cu), Fig. 11(b), the residual surface strain is much smaller ($\epsilon \sim 0.3$).

This key difference in the surface strain produced when cutting an annealed metal vs a hardened metal is the origin of a somewhat curious chip-formation phenomenon—flow and chip thickness oscillations during cutting. Figure 12 shows images of chips created in successive revolutions when turning annealed Cu. These images are extracted from a high speed *in situ* sequence. The striking difference

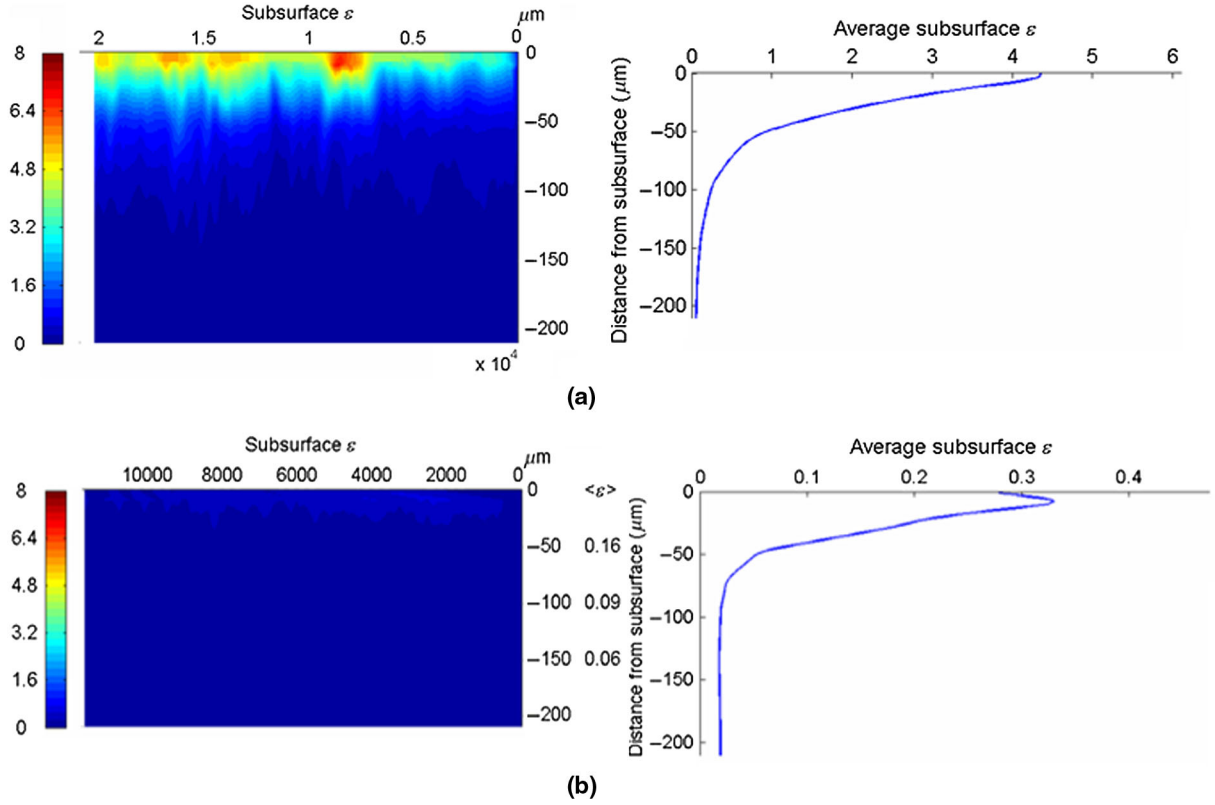

FIG. 11. Residual strain on workpiece surface for (a) annealed Cu and (b) hardened Cu. The images on the left show the strain distribution on the cut surface, while the plots on the right show the average strain as a function of depth. For the annealed case, the sinuous flow with folding results in large strains (>3) on the newly formed workpiece surface. By contrast, a very small strain (approximately equal to 0.3) is seen in the hardened case (at −50 μm) due to the absence of folding.

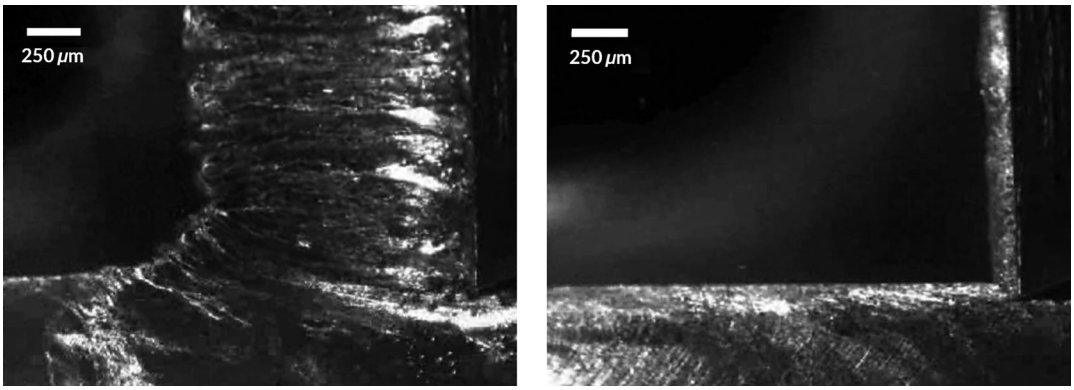

FIG. 12. Chip-thickness oscillations in the rotary cutting of annealed Cu. (Left panel) When cutting over an annealed layer, sinuous flow occurs and a thick chip is formed. In the second pass (right panel), cutting occurs over a strain-hardened region resulting in laminar flow and a very thin chip.

between the two chips is in their thickness: the chip in Fig. 12(a) is about 5 times as thick as the chip in Fig. 12(b), even though both chips are produced nominally from the same annealed Cu. Video 2 shows the complete image sequence of this chip formation over two revolutions of the workpiece. This pattern of oscillating chip thickness, alternating between thick and thin chips with a frequency matching the rotation of the workpiece, is found to repeat over many revolutions.

The thickness oscillations are due to the operative flow mode, and the dependence of this mode on the initial state of the material being cut. In the first revolution of the cutting, the Cu surface is in the annealed condition and sinuous flow occurs, with a thick chip having the mushroom morphology [Fig. 12(a)]. Because of this flow, the workpiece surface is severely strained [$\epsilon \sim 4$; Fig. 11(a)] to a depth of about -50 μm (roughly h_0). Hence, the initial workpiece surface is a prestrained state for the next cutting revolution. The laminar flow mode now prevails and a thin chip results [Fig. 12(b)]. The newly generated surface left behind after this revolution is only minimally strained [$\epsilon \sim 0.3$; Fig. 11(b)]. As a result, the workpiece surface is once again in a near-annealed state for the following (third) cutting cycle and a thick chip is formed by sinuous flow. This back-and-forth oscillation between sinuous and laminar flow, with corresponding oscillations in chip thickness, is found to occur over many workpiece revolutions when cutting annealed Cu.

VIDEO 2. Chip-thickness oscillation during the cutting of Cu.

These observations linking the initial material state, type of plastic flow, and residual surface strain suggest the unique possibility of preparing strain-free surfaces by cutting. It is well known that cutting and finishing operations (at small h_0) result in a subsurface layer with some residual plastic strain and a refined microstructure. In our work, the thickness of this layer is measured as being roughly h_0 [Fig. 11(a)]. For applications where a strain-free surface is desirable, this finding suggests the use of a two-pass cutting process. Following the first cutting pass, the value of h_0 for the second pass is adjusted to match the depth of the residual strain zone on the workpiece surface. Consequently, in the second pass, material removal occurs by laminar plastic flow. Then, as shown in Fig. 12(b) for Cu, a near strain-free surface results on the workpiece surface. Similar strain-free surfaces are produced in Al.

IV. DISCUSSION

The *in situ* observations demonstrate that the cutting of metals can be mediated by a type of unsteady flow that is quite different from the well-known laminar and shear-band flow modes. This unsteady flow, termed sinuous flow, is characterized by repeated material folding (see Fig. 5); hence, this flow can effect very large shape transformations (see, e.g., Fig. 2) that are likely not achievable by the laminar flow. Our observations show that sinuous flow is quite prevalent in the simple shearing of annealed metals with varied microstructures, such as Cu, Al, and brass 260, which possess significant workability. Sinuous flow can be considered as a collective mesoscopic mode of large-strain plastic deformation in the same genre as laminar flow [2], shear banding [7,10], and kinking [23]. This type of

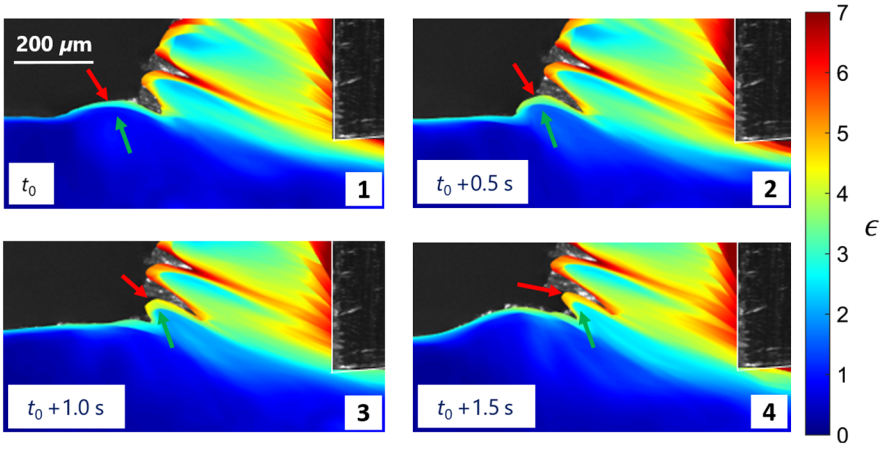

FIG. 13. Gradient in strain due to the buckling deformation governing bump formation. The red arrow points to an outer fiber which undergoes higher strain than the inner fibers (the green arrow). $h_0 = 50$ μm, $V_0 = 0.5$ mm/s.

unsteady flow is the reason why annealed metals, although soft, are very much more difficult to cut (large forces, very thick chip, and extensive side flow) when compared to the same metals in an initially hardened state.

A. Plastic buckling and the role of material microstructure

The direct observations capture the initiation and development phases of the sinuous flow in Cu (Fig. 6) and Al (Fig. 7), and they highlight the mechanics of this flow development involving folding. Fold initiation occurs by the formation of a bump on the workpiece surface ahead of the tool (Fig. 6), driven by the compressive field in this region. As the tool advances, this bump grows in height between pinning points in a manner very similar to the plastic buckling of a compressed pinned column [29]. These pinning points are typically grain boundaries in the pure metals.

Evidence for local plastic buckling of material on the free surface is also provided by the *in situ* observations. Buckling and bending of beams and columns are characterized by strain gradients from the convex to the concave side of the bending column. This gradient in strain is clearly observed in Fig. 13. The figure shows four frames from a high-speed sequence, delineating the formation of a single fold (between the red and green arrows). The instantaneous material strain, obtained from PIV, is overlaid on each of the frames. Beginning with the bump initiation (time t_0, frame 1), the strain distribution in the vicinity of the incipient fold shows a gradient from the free surface (convex side, red arrow) to the material interior (concave side, green arrow). In fact, this gradient is amplified as the fold enters the chip (frame 3) and results in the inhomogeneous strain field and microstructure in the chip (frame 4). Additionally, surface plastic buckling of a similar type has been observed in a class of shear- and tube-spinning processes [33], which employ a very similar deformation geometry, albeit without chip formation. In these processes, the buckling can even lead to delamination of the component being spun from the mandrel on which it is mounted. In fact, this buckling is a key process limit [34].

The fact that the pinning points correspond to material heterogeneities is revealed by grain-level imaging. Figure 14 shows three frames from a high-speed image sequence of the cutting of annealed Cu. Here, the individual grains are revealed by thermally etching Cu [31,35] prior to cutting, allowing the dynamics of individual grains to be

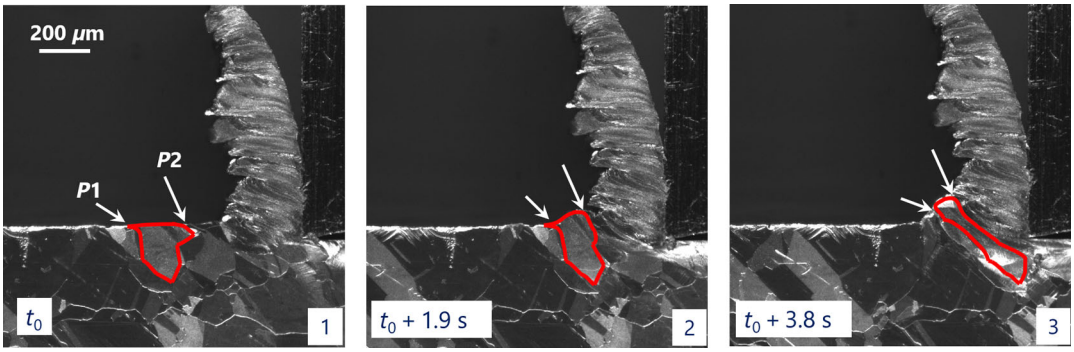

FIG. 14. Frames from an image sequence showing the microstructural basis for plastic buckling and sinuous flow. The pinning points P_1 and P_2 (frame 1) correspond to grain boundaries. The single grain (highlighted in red) undergoes plastic buckling to form a bump (the arrows, frame 2). With subsequent shearing and rotation, this bump evolves to form a single fold (frame 3).

tracked *in situ* during deformation. The extremities of the initial bump are clearly seen to be located at the grain boundaries (frame 1). The fact that the extremities of the bump are located at grain-boundaries is confirmed by an analysis of 25 bumps from similar image sequences; approximately 75% of these bumps had surface grain-boundaries as pinning points. In the remaining cases, it is likely that out-of-plane grain boundaries form the pinning points and are therefore not visible in the plane of observation. The images also reveal the connection between fold size and material grain size and the development of mushroomlike features on the chip surface. A bump amplifies in size as it approaches the tool (frame 2). With further shearing, it develops into a highly elongated grain (frame 3), with the free surface of the grain distorted into a mushroom-shaped cap. Each fold in the chip is composed of one or a few deformed grains. The broad distribution of fold widths arises from intrinsic grain-size variations in the annealed Cu. In addition, the strong orientation dependence of flow stress and elastic properties of the Cu grains are known to induce folding [25,36].

While fold formation is influenced by the location of grain boundaries, the occurrence of sinuous flow itself is not restricted to cases with a large grain size. As an illustrative example, Fig. 15 shows the cutting of annealed Cu, with a grain size of 50 μm, an order of magnitude smaller than the grain sizes in other experiments (500 μm). The streaklines superimposed on the image clearly show the sinuous flow mode to still be operative. Coupled with similar observations in other systems, such as Al, pure Fe (ARMCO), and low-carbon steels, it is clear that sinuous flow is the predominant mode of deformation for a range of conditions (e.g., grain size) in ductile metals.

The nucleation of the bumps by the plastic buckling of thin layers on the workpiece surface ahead of the tool offers

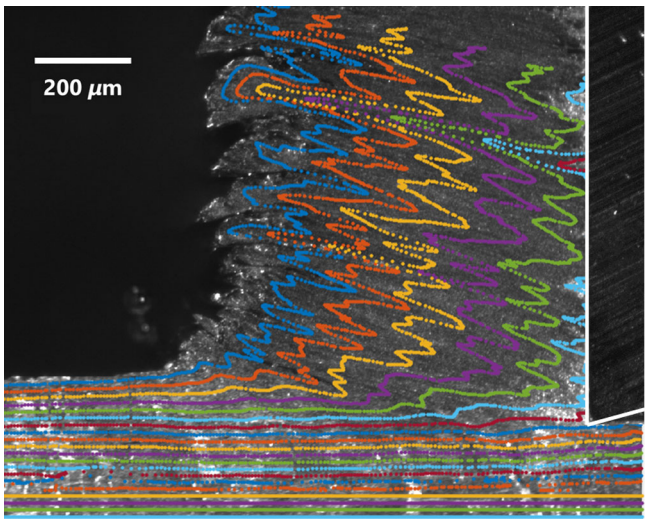

FIG. 15. Cutting of annealed Cu with a grain size of 50 μm. One frame from a high-speed sequence shows wavy streaklines reflecting sinuous flow. $V_0 = 0.42$ mm/s.

clues to the mechanics of sinuous-flow development. Sinuous flow is triggered by a plastic surface instability, with material heterogeneities determining the location where this instability first occurs. In other words, the relative stability of flow modes determines which mode is operative in large-strain deformation. Such an analysis is beyond the scope of this study but is considered in a separate publication [31].

B. Transition from laminar to sinuous flow

Three points are worthy of mention with regard to transitions from laminar flow to sinuous flow. First, the observations show that flow stability in large-strain deformation can be controlled by merely varying the initial deformation state of the metal: an annealed state promotes sinuous flow, while a hardened state is conducive to laminar flow for the same deformation geometry. Flow stability is also affected by a change in the deformation geometry—we observe that stable laminar flow can be established even in annealed metals by making the tool angle α moderately positive (e.g., 45°). It is thus imperative that, for accurate modeling of the cutting, even for simple annealed metals with well-defined constitutive (mechanical) properties, careful consideration be given to the stability of flow modes and the role of material heterogeneity (e.g., grain boundary and second phases) in guiding the flow evolution [37]. While a few stability analyses of cutting have been done, these have been carried out largely in the framework of the shear-plane model [15–17] and, hence, are questionable. *In situ* observations, as in this study, can be of value in formulating and validating stability analyses.

Second, the shear-plane (laminar-flow) models of chip formation have generally been based on a hypothesis of minimal energy dissipation in cutting. While applications of minimum-energy hypotheses to highly dissipative deformation processes such as metal cutting are questionable—and have been criticized sufficiently [38,39]—it is nevertheless instructive to use the flow field data from the *in situ* observations and to then compare the energy dissipation for laminar and sinuous flow. The simple computations in Sec. III D have shown that sinuous flow, despite the extensive folding, requires much less energy than laminar flow to effect the same chip shape transformation in annealed Cu. Thus, the material appears to select a flow mode that results in lower energy dissipation. A selection of flow mode based on some sort of minimum-energy principle appears to prevail with sinuous vs laminar flow in the manner of Merchant [2].

Third, a flow transition from laminar to vortexlike flow, similar to that observed here, has also been noted at much smaller length scales. This is the transition from laminar to rotational dislocation plasticity [40], the latter being characterized by vortex features similar to those of the sinuous flow, but with different underlying physics. Additionally,

reports of atomistic numerical simulations and associated experiments using AFM tips [41–44] have indicated the occurrence of folding-type flow features in polycrystalline metals on the nanoscale. However, these phenomena occur at the lattice or grain level; closer to the length scale of interest for the present observations (10–100 μm) is a highly rotational flow seen in the sliding of metals which mediates a type of folding, and surface defects (e.g., cracks and tears) and wear particles [25]. An examination of this sliding flow suggests that it is a milder version of the sinuous flow in cutting, with microstructure heterogeneity again influencing the folding.

C. Conditions favoring sinuous flow

The conditions promoting sinuous flow can now be summarized. These are a propensity for material to undergo large-strain plastic deformation; a deformation geometry with minimal constraints to the flow, as near a free surface, and which promotes large-strain deformation; and suitable material heterogeneities like grains and second phases. Sinuous flow can thus be expected in material systems such as pure metals, Ni alloys, stainless steels, mild steel, and even ductile polymers. In fact, we have very recently observed this flow in the cutting of polypropylene. Deformation configurations that should facilitate sinuous flow are cutting, sliding, and surface deformation processes like peening, burnishing, and shear spinning.

D. Flow effects on surface quality

Sinuous flow—like another nonhomogeneous flow mode, shear banding—should have undesirable consequences for component surface quality in manufacturing processes. The large forces can cause chatter vibrations with adverse consequences for dimension control and surface finish. The nonhomogeneous nature of this flow could result in variations in strain, microstructure, and mechanical properties along the workpiece length, as well as delamination defects (e.g., tears, smears, and cracks) [25]. Even absent chatter vibration, the finish on cut surfaces of annealed Cu (sinuous flow) is found to be inferior to that on surfaces of hardened Cu (laminar flow). Also, as discussed, the machined surface in annealed Cu is severely deformed compared to that in hardened Cu (Fig. 11); this severe straining will adversely impact the fatigue and wear behavior of structural components.

From a manufacturing quality standpoint, sinuous flow is, therefore, to be avoided. Our observations of how sinuous flow is nucleated suggest material-agnostic approaches for suppressing this flow even in annealed metals. One of these approaches is cutting with a tool of positive α, a deformation geometry that stabilizes laminar flow by inhibiting the surface buckling. A second approach, based on the propensity for laminar flow in hardened Cu, is to carry out a preliminary cutting pass with a small h_0 value so as to prestrain the surface before the final cutting. This approach is also suggested by the chip-thickness-oscillation phenomenon seen in the cutting of annealed Cu. Third, as with structural columns, bump nucleation (buckling) could be suppressed by constraining the workpiece surface just ahead of the tool. This approach has worked well in cutting experiments; when an auxiliary die is placed across from the tool to locally constrain the annealed Cu surface, laminar flow results. In all instances where sinuous flow is reduced or suppressed, the surface quality attributes improve, and cutting forces are reduced, sometimes by as much as 50% (see Fig. 3).

Finally, our results also offer the additional possibility of producing strain-free metal surfaces by two-pass cutting, as is discussed and demonstrated in Sec. III F.

E. Implications for modeling of large-strain deformation

The occurrence of sinuous flow in annealed metals of commercial purity, whose large-strain deformation behavior is among the best characterized in terms of constitutive mechanical properties, raises questions with regard to predictions of output variables in material removal and tribological processes. Clearly, this type of flow cannot be accommodated within the framework of slip-line field and upper-bound models of plasticity, as these models are based on assumptions of smooth homogeneous deformation. What about finite-element (FE) modeling, however, which has become the preferred method to analyze machining and forming processes in recent years?

An examination of predictive claims of FE models shows that their validation has been based largely on reproducing numerical values of ensemble parameters such as forces, and less so on phenomenological and quantitative details of flow and deformation [45,46]. We are not aware of any FE predictions of deformation in cutting that bear even a slight resemblance to the sinuous flow highlighted in this study. Discrepancies in FE predictions have often been attributed to uncertainty in constitutive material property data at large strains and strain rates, and to friction conditions at cutting interfaces. Since such property data for commercially pure metals like Cu and Al are well established and the present observations of sinuous flow are actually made for small-strain-rate ($<200\ s^{-1}$) cutting, it appears that there is much that still remains to be done on the modeling front—even at the continuum scale.

The present observations bring to the fore a need for continuum models to incorporate flow-stability considerations, microstructure heterogeneity at the micrometer length scale, and a definition of the initial deformation state of the workpiece so that deformation aspects of machining can be properly predicted. A possible way for including microstructure in a FE framework is via Voronoi-cell partitioning of the surface, where each cell represents a grain with distinct flow properties reflecting its anisotropy. Modeling microstructure heterogeneity within such a

continuum framework has enabled experimenters to quantitatively reproduce the effects of folding under large-strain deformation [25,47,48].

A likely casualty of this study is the smooth-flow model for the cutting of ductile metals proposed more than 70 years ago and still widely used [2]. The prototypical examples of such metals are annealed metals, especially the annealed Cu and Al studied here. As the present observations have shown, sinuous flow dominates in these metals [1,2]. A reexamination of the foundations of metal cutting and of modeling of large-strain deformation at surfaces is therefore warranted.

V. CONCLUSIONS

In this work, we study the large-strain plastic deformation of ductile, annealed metals in simple shear by cutting using high-speed *in situ* imaging and image analysis. The deformation at the mesoscale is found to be highly nonuniform and mediated by a flow mode with significant rotation components—sinuous flow. This flow results in chip formation by large-amplitude folding and very large shape changes. The observations contradict the oft-used description of large-strain deformation in these metals as having arisen from smooth uniform flow. The nucleation and development phases of the sinuous flow, the fold characteristics, and the energy dissipation for shape change are characterized quantitatively. Sinuous flow is confirmed to be a general mesoscopic surface flow mode in annealed metals, in the same genre as kinking and shear banding, with the capability of effecting very large shape changes. A phenomenological mechanism rooted in plastic buckling and grain-level heterogeneity is proposed to describe this flow. The occurrence of the sinuous flow mode further reinforces the critical role of stability of plastic flow in selecting the deformation mode in the cutting and deformation processing of metals. It explains why soft annealed metals are so much more difficult to cut than the same metals in hardened states. That chip formation could occur by folding in these metals, a deformation pattern bearing little resemblance to the classical shear-zone model for cutting, is most unexpected.

ACKNOWLEDGMENTS

The authors would like to acknowledge support from U.S. Army Research Office Grant No. W911NF-15-1-0591, NSF Grants No. CMMI 1562470 and DMR 1610094, and the U.S. Department of Energy EERE program via Award No. DE-EE0007868.

[1] M. C. Shaw, *Metal Cutting Principles* (Oxford University Press, New York, 2005).

[2] M. E. Merchant, Mechanics of the metal cutting process. I. Orthogonal cutting and a type 2 chip, J. Appl. Phys. **16**, 267 (1945).

[3] V. Piispanen, Theory of formation of metal chips, J. Appl. Phys. **19**, 876 (1948).

[4] K. Okushima and K. Hitomi, On the cutting mechanism for soft metals, Memoirs of the Faculty of Engineering, Kyoto University **19**, 135 (1957).

[5] P. Oxley, Mechanics of metal cutting, Int. J. Mach. Tool Des. Res. **1**, 89 (1961).

[6] V. P. Kravz-Tarnavskii, A peculiar band discovered in steel (in Russian), Z. Russ. Metall. **3**, 162 (1928).

[7] C. Zener, in *Fracturing of Metals* (American Society for Metals, Cleveland, 1948), p. 3.

[8] B. Dodd, S. M. Walley, R. Yang, and V. F. Nesterenko, Major steps in the discovery of adiabatic shear bands, Metall. Mater. Trans. A **46**, 4454 (2015).

[9] S. D. Antolovich and R. W. Armstrong, Plastic strain localization in metals: Origins and consequences, Prog. Mater. Sci. **59**, 1 (2014).

[10] R. F. Recht, Catastrophic thermoplastic shear, J. Appl. Mech. **31**, 189 (1964).

[11] K. Nakayama, in *Proceedings of the International Conference on Production Engineering, Tokyo, 1974* (Japan Society of Precision Engineering, Tokyo, 1974), p. 572.

[12] D. Sagapuram, K. Viswanathan, A. Mahato, N. K. Sundaram, R. M'Saoubi, K. P. Trumble, and S. Chandrasekar, Geometric flow control of shear bands by suppression of viscous sliding, Proc. R. Soc. A **472**, 20160167 (2016).

[13] T. J. Burns and M. A. Davies, Nonlinear Dynamics Model for Chip Segmentation in Machining, Phys. Rev. Lett. **79**, 447 (1997).

[14] R. Komanduri and B. Von Turkovich, New observations on the mechanism of chip formation when machining titanium alloys, Wear **69**, 179 (1981).

[15] R. Hill, On the limits set by plastic yielding to the intensity of singularities of stress, J. Mech. Phys. Solids **2**, 278 (1954).

[16] R. Hill, The mechanics of machining: A new approach, J. Mech. Phys. Solids **3**, 47 (1954).

[17] A. Molinari and A. Moufki, The merchant's model of orthogonal cutting revisited: A new insight into the modeling of chip formation, Int. J. Mech. Sci. **50**, 124 (2008).

[18] H. Yeung, K. Viswanathan, W. D. Compton, and S. Chandrasekar, Sinuous flow in metals, Proc. Natl. Acad. Sci. U.S.A. **112**, 9828 (2015).

[19] J. E. Williams, E. F. Smart, and D. R. Milner, Metallurgy of machining. Part 1: Basic considerations and the cutting of pure metals, Metallurgia **81**, 3 (1970).

[20] K. Viswanathan, A. Udupa, H. Yeung, D. Sagapuram, J. B. Mann, M. Saei, and S. Chandrasekar, On the stability of plastic flow in cutting of metals, CIRP Ann. **66**, 69 (2017).

[21] P. K. Wright, Predicting the shear plane angle in machining from workmaterial strain-hardening characteristics, J. Eng. Ind. **104**, 285 (1982).

[22] J. T. Black, On the fundamental mechanism of large strain plastic deformation: Electron microscopy of metal cutting chips, J. Eng. Ind. **93**, 507 (1971).

[23] E. Orowan, A type of plastic deformation new in metals, Nature (London) **149**, 643 (1942).
[24] T. Atkins, *The Science and Engineering of Cutting* (Butterworth-Heinemann, Washington, DC, 2009).
[25] N. K. Sundaram, Y. Guo, and S. Chandrasekar, Mesoscale Folding, Instability, and Disruption of Laminar Flow in Metal Surfaces, Phys. Rev. Lett. **109**, 106001 (2012).
[26] R. J. Adrian and J. Westerweel, *Particle Image Velocimetry*, Cambridge Aerospace Series Vol. 30 (Cambridge University Press, Cambridge, England, 2010).
[27] A path line, the trajectory along which an individual particle (material point) travels, is useful for analyzing strain accumulation, while a streakline, the locus of all particles that have passed earlier through a particular spatial point, is valuable for flow visualization.
[28] S. Ramalingam, E. D. Doyle, and D. M. Turley, On chip curl in orthogonal machining, J. Eng. Ind. **102**, 177 (1980).
[29] F. R. Shanley, Inelastic column theory, J Aeronaut Sci **14**, 261 (1947).
[30] J. G. Ramsay and M. I. Huber, *Modern Structural Geology, Volume 2: Folds and Fractures* (Academic Press, London, 1987).
[31] A. Udupa, K. Viswanathan, Y. Ho, and S. Chandrasekar, The cutting of metals via plastic buckling, Proc. R. Soc. A **473**, 20160863 (2017).
[32] G. R. Johnson and W. H. Cook, in *Proceedings of the 7th International Symposium on Ballistics, The Hague, Netherlands, 1983*, Vol. 21 (International Ballistics Society, 1983), p. 541.
[33] S. Kalpakjian and S. Rajagopal, Spinning of tubes: A review, Journal of applied metalworking **2**, 211 (1982).
[34] W. A. Backofen, Deformation processing, Metall. Trans. **4**, 2679 (1973).
[35] W. W. Mullins, Theory of thermal grooving, J. Appl. Phys. **28**, 333 (1957).
[36] S. Dub, Y. Lim, and M. Chaudhri, Nanohardness of high purity Cu (111) single crystals: The effect of indenter load and prior plastic sample strain, J. Appl. Phys. **107**, 043510 (2010).
[37] J. R. Rice, in *Proceedings of the 14th International Congress on Theoretical and Applied Mechanics, Delft, Netherland, 1976*, edited by W. T. Koiter (North-Holland, Amsterdam, 1976), p. 207.
[38] H. L. D. Pugh, in *Proceedings of the Conference on Technology of Engineering Manufacture, London, 1958* (Institution of Mechanical Engineers, London, 1958), p. 237.
[39] P. Dewhurst, On the non-uniqueness of the machining process, Proc. R. Soc. A **360**, 587 (1978).
[40] L. M. Brown, Transition from laminar to rotational motion in plasticity, Phil. Trans. R. Soc. A **355**, 1979 (1997).
[41] N. Beckmann, P.A Romero, D. Linsler, M. Dienwiebel, U. Stolz, M. Moseler, and P. Gumbsch, Origins of Folding Instabilities on Polycrystalline Metal Surfaces, Phys. Rev. Applied **2**, 064004 (2014).
[42] Q. Li, Y. Dong, D. Perez, A. Martini, and R. W. Carpick, Speed Dependence of Atomic Stick-Slip Friction in Optimally Matched Experiments and Molecular Dynamics Simulations, Phys. Rev. Lett. **106**, 126101 (2011).
[43] A. Li and I. Szlufarska, How grain size controls friction and wear in nanocrystalline metals, Phys. Rev. B **92**, 075418 (2015).
[44] X.-Z. Liu, Z. Ye, Y. Dong, P. Egberts, R. W. Carpick, and A. Martini, Dynamics of Atomic Stick-Slip Friction Examined with Atomic Force Microscopy and Atomistic Simulations at Overlapping Speeds, Phys. Rev. Lett. **114**, 146102 (2015).
[45] T. Marusich and M. Ortiz, Modelling and simulation of high-speed machining, Int. J. Numer. Methods Eng. **38**, 3675 (1995).
[46] V. Madhavan, S. Chandrasekar, and T. Farris, Machining as a wedge indentation, J. Appl. Mech. **67**, 128 (2000).
[47] N. K. Sundaram, A. Mahato, Y. Guo, K. Viswanathan, and S. Chandrasekar, Folding in metal polycrystals: Microstructural origins and mechanics, Acta Mater. **140**, 67 (2017).
[48] A. Vandana and N. K. Sundaram, Interaction of a sliding wedge with a metallic substrate containing a single inhomogeneity, Tribol. Lett. **65**, 124 (2017).